Journal of Geospatial Surveying (2026) 6:1
DOI: 10.4038/jgs.v6i1.72

ORIGINAL ARTICLE

Integrated Geospatial Feature Extraction and Land Mapping of Eastern India Using High-Resolution Satellite Data

Kumar, A. *[a], Daimary, R. [b], Kumar, R. [c]

[a] Department of Computer Science & Engineering, Manipal University Jaipur, Rajasthan, India

[b] Department of Media, Communication and Fine Arts, Manipal University Jaipur, Rajasthan, India

[c] School of Communication, Amity University Ranchi, Jharkhand, India

ARTICLE INFO

Article history:
Received 25 July 2025
Received in revised form 3 November 2025
Accepted 28 November 2025
Available online 02 January 2026

Keywords:
Georeferencing and Digitization
False Color Composite
Image Preprocessing and Noise Reduction
Geospatial Feature Extraction
High-Resolution Satellite Imagery

ABSTRACT

This study presents a comprehensive approach to extracting geospatial features from high-resolution satellite imagery of a terrestrial region located in eastern India. The analysis employed remotely sensed data acquired through the European Space Agency (https://www.esa.int/). The raw radiance data were pre-processed to generate geophysical parameters encompassing atmospheric, oceanic, and terrestrial domains. Satellite imagery underwent radiometric correction, noise reduction, and contrast enhancement to improve visual and analytical quality. Adaptive median filtering techniques were applied to suppress artifacts introduced during image acquisition, ensuring the preservation of true pixel intensity patterns. False colour composites constructed from red, near infrared, and short-wave infrared spectral bands facilitated detailed land cover identification and classification. Georeferencing and precise on-screen digitisation were performed to produce accurate thematic layers. The resulting geodatabase serves as a valuable resource for quantitative assessments and automated report generation, supporting effective evaluation of land resources and environmental monitoring.

1 Introduction

Remote sensing has become an indispensable tool for geospatial monitoring, particularly with the emergence of very high spatial resolution satellite imagery (Kumar, 2020; Kumar, 2023; Kumar et al., 2024a; Kumar and Gorai, 2022; Kumar and Prasad, 2023). Among the most powerful satellite systems in this domain is QuickBird, a commercial earth observation satellite operated by DigitalGlobe, offering sub-meter resolution and multispectral capabilities. QuickBird's panchromatic sensor provides a spatial resolution of 0.61 m at nadir and up to 0.66 m off-nadir, while its multispectral sensor offers 2.44 m to 2.88 m resolution (Toutin, 2009). This fine spatial detail enables the discrimination of small land cover features and supports applications in urban planning, disaster response, forestry, biodiversity assessment, and environmental change monitoring (Daimary et al., 2024; Daimary and Kumar, 2024; Kumar et al., 2024b; Kumar et al., 2024c; Kumar and Rathee, 2017; Kumar and Villuri, 2015). In the context of the Sundarbans region, located in the eastern part of India, remote sensing is vital. The Sundarbans, United Nations Educational, Scientific and Cultural Organisation (UNESCO) World Heritage site, comprises over 10,000 km² of deltaic terrain and mangrove ecosystems, spanning southern West Bengal and parts of Bangladesh. This ecologically fragile area is highly sensitive to environmental stressors such as sea-level rise, cyclonic storms, land erosion, and anthropogenic pressure. Rapid urbanisation and unsustainable land use practices have led to severe degradation of natural habitats (Daimary and Chetia, 2025; Daimary and Deka, 2025; Giri et al., 2015). Accurate and high-resolution spatial information is essential for sustainable management of the region's natural resources (Kumar et al., 2026; Ojha et al., 2024). QuickBird's multispectral sensor covers four spectral bands: blue (0.45–0.52 μm), green (0.52–0.60 μm), red (0.63–0.69 μm), and near-infrared (NIR) (0.76–0.90 μm). These bands are optimal for analyzing vegetation health, water bodies, built-up areas, and soil moisture conditions. The satellite has a revisit time of 1–3.5 days, ensuring temporal consistency for time-series analysis (Jensen, 1996). Object-Based Image Analysis (OBIA) is a preferred approach for analysing such high-resolution data, where segmentation algorithms divide imagery into homogenous regions or "image-objects" which are then classified using

* Corresponding author: A. Kumar, Department of Computer Science & Engineering, Manipal University Jaipur, Rajasthan, India.

E-mail address: ajay3789@gmail.com (A. Kumar).

spatial, spectral, and contextual attributes (Blaschke, 2010; Kumar et al., 2023; Paygude et al., 2024). The OBIA approach is critical in overcoming the limitations of pixel-based classification, especially when working with high-resolution imagery where spectral variation within classes can be high (Kumar, 2024; Kumar and Gorai, 2022; Kumar et al., 2022). The segmentation process uses spatial filters, histogram analysis, and edge-detection techniques to define object boundaries. Image preprocessing steps include radiometric correction, noise filtering (e.g., adaptive median filters with kernel size 3×3 or 5×5), and enhancement using Principal Component Analysis (PCA) or contrast stretching (Richards and Jia, 2006). High-resolution imagery also enables the mapping of impervious surfaces, which is essential in urban studies (Kumar and Gorai, 2023a; Kumar and Gorai, 2023b; Kumar and Gorai, 2023c). Impervious surfaces, such as roads, rooftops, and pavements, are indicators of urbanisation and contribute to hydrological changes, including reduced infiltration and increased surface runoff. Previous studies have demonstrated a strong correlation ($R^2 > 0.85$) between the extent of impervious surfaces and urban growth metrics (Weng, 2012). By leveraging QuickBird's 0.61 m resolution, even narrow features can be delineated with a positional accuracy of ±2 m post-georeferencing.

Despite the advancements in remote sensing and the availability of high-resolution data, there exists a significant research gap in:

(a) Feature-Level Classification Accuracy: Many studies still rely on pixel-based methods or coarse-resolution imagery (10–30 m), which are insufficient for detailed urban, agricultural, and mangrove feature mapping in complex landscapes like the Sundarbans.

(b) Integration of OBIA with High-Resolution Imagery in Sensitive Ecological Zones: While OBIA has proven its effectiveness globally, its application in the Sundarbans region using QuickBird data remains limited in the literature. There is a lack of integrated frameworks that combine OBIA, spectral indices, and multi-temporal change detection to monitor the intricate land cover patterns of this biosphere reserve.

(c) Noise Reduction and Spectral Correction at High Resolution: Digital imagery, particularly from high-resolution satellites, is prone to noise caused by sensor errors, atmospheric interference, and platform instability. There is insufficient documentation on optimised filtering techniques tailored to QuickBird's data characteristics.

(d) Data Fusion and Automated Reporting: Though large-scale mapping is enabled by satellites like QuickBird and GeoEye-1, there is minimal use of automated report generation, spatial databases, and integration with GIS for decision-making. Most analyses are visual or static, lacking the computational depth needed for real-time monitoring or alert systems.

(e) Spectral Confusion in Urban-Agricultural-Mangrove Interfaces: The Sundarbans region presents a challenge due to the close spatial juxtaposition of agricultural land, mangroves, and expanding urban areas. This leads to spectral confusion in traditional classifiers, especially when land parcels are smaller than 10 m^2. There is a need for context-aware algorithms that incorporate shape, texture, and spectral signatures concurrently.

The Sundarbans, a region marked by ecological fragility and high population density, faces escalating pressure from environmental degradation, urban encroachment, and the impacts of climate change. Efficient planning, resource allocation, and conservation strategies demand accurate, high-resolution spatial data to inform decisions. However, traditional methods relying on medium-resolution imagery (e.g., Landsat 30 m, MODIS 250–500 m) are inadequate for mapping fine-scale features, particularly in heterogeneous landscapes. The key problems that necessitate investigation are:

(a) Lack of fine-scale feature extraction frameworks: Current remote sensing workflows are not optimised for detecting micro-level land features (<1 m width) such as small aquaculture ponds, narrow roads, or fragmented mangrove patches.

(b) Inadequate spectral-spatial analysis in data-rich environments: Although QuickBird provides superior spatial and spectral resolution, existing workflows often under-utilise its full potential due to inefficient segmentation, classification, and noise-filtering pipelines.

(c) Absence of an integrated OBIA framework for Sundarbans: The region lacks a dedicated object-based geospatial framework tailored to high-resolution imagery that can accurately extract and monitor features relevant to ecology, urbanisation, and land-use dynamics.

(d) Data noise and misclassification risks: High-resolution imagery is vulnerable to radiometric noise and misclassification due to high within-class spectral variability. Without precise filtering and enhancement techniques, this leads to unreliable land cover maps.

(e) Low adoption of georeferenced databases and automated analysis: Manual interpretation and static maps dominate decision-making processes. There is minimal use of geospatial databases and report generation systems that can integrate temporal analyses, field data, and spectral indicators.

1.1 Related Work and Literature Review

The comprehensive review of existing methodologies and advancements is succinctly summarised in Table 1, highlighting the core strengths, limitations, and numerical benchmarks across each thematic domain. This structured synthesis offers a clearer understanding of the evolving landscape of high-resolution geospatial feature extraction, emphasising the critical need for integrated, accurate, and automated approaches in complex terrestrial environments.

(a) High-Resolution Satellite Imagery for Feature Extraction: High-resolution satellite imagery (HRSI) plays a crucial role in mapping micro-terrain elements and land cover heterogeneity. Platforms such as QuickBird (0.61 m PAN, 2.44–2.88 m MS), WorldView-2 (0.46 m PAN, 1.84 m MS), and GeoEye-1

(0.41 m PAN, 1.65 m MS) have demonstrated capabilities in capturing sub-meter details essential for urban and ecological studies (Zhou, 2020). Notably, QuickBird data have been widely used in the identification of small-scale features such as rooftops, canals, and vegetative patches as small as 1–2 m^2 (Toutin, 2009).

(b) OBIA: The OBIA paradigm is particularly suited for very high-resolution imagery where pixel-based approaches yield high misclassification due to spectral confusion. Blaschke (2010) demonstrated that OBIA reduces classification errors by 15–30% in heterogeneous landscapes compared to traditional maximum likelihood classifiers. When applied to QuickBird imagery, segmentation with multiresolution algorithms at scale parameters of 20–50 enables delineation of landscape elements smaller than 0.5 ha (Chen et al., 2012). OBIA utilises shape descriptors, texture metrics (e.g., GLCM variance greater than 50), and spectral indices, such as NDVI, NDBI, and NDWI, for feature classification.

(c) Radiometric and Geometric Correction: Radiometric distortions due to atmospheric scattering and sensor-induced noise significantly impact high-resolution images. Adaptive median filters (kernel sizes 3×3, 5×5) have proven effective in mitigating Gaussian and salt-and-pepper noise, improving SNR by up to 8–10 dB (Richards and Jia, 2006). Georeferencing accuracy is critical; RMSE values < 5 m are acceptable for feature extraction in sub-meter imagery, achievable via ground control point (GCP) integration and polynomial transformations (Aguilar et al., 2007).

(d) False Colour Composites (FCC) and Spectral Band Usage: FCCs combining Red, NIR, and SWIR bands enhance vegetation delineation and moisture detection. NIR (0.76–0.90 μm) is particularly helpful in assessing biomass and mangrove health due to its chlorophyll reflectance, while SWIR (1.55–1.75 μm) highlights soil and urban surfaces. Use of FCC improved land cover separation accuracy by 12–17% compared to true colour composites (Jensen, 1996).

(e) Applications in the Sundarbans and Similar Coastal Regions: Giri et al. (2015) used Landsat (30 m) and MODIS (250 m) to map mangrove extent in the Sundarbans. However, such coarse data resulted in omission errors of more than 20% for fragmented patches. In contrast, QuickBird and WorldView-2 facilitated mapping of features <10 m^2 with overall accuracy exceeding 90% when OBIA and post-classification refinement were applied (Zhang et al., 2021). Still, studies combining OBIA with spectral indices and temporal monitoring for the Sundarbans are sparse.

Table 1: Reviewed literature: sensors, methods, aim, and accuracy.

Author(s)	Sensor / Resolution	Methodology	Target Features	Accuracy	Remarks
Toutin (2009)	QuickBird (0.61 m PAN, 2.44 m MS)	OBIA, Spectral Indexing	Urban, water, vegetation	>90%	High revisit, useful for urban planning
Blaschke (2010)	Multiple HRSI	OBIA, Multiresolution segmentation	Mixed landscapes	15–30% error reduction	Contextual analysis key for HRSI
Richards and Jia (2006)	Simulated HRSI	Adaptive filtering, PCA	Noise removal, enhancement	SNR ↑ by 8–10 dB	PCA enhances contrast in NIR and Red bands
Giri et al. (2015)	Landsat (30 m), MODIS (250 m)	Pixel-based classification	Mangrove coverage	Omission >20%	Coarse resolution unsuitable for fragmented features
Zhang et al. (2021)	WorldView-2 (0.46 m PAN)	OBIA + Random Forest	Mangrove, agriculture, urban edges	94–96%	Advanced classifier increases robustness
Chen et al. (2012)	QuickBird	OBIA + GLCM Texture	Urban-mixed land uses	>88%	Texture enhances classification in built-up areas
Wu et al. (2015)	HRSI	Polynomial georeferencing	General land cover	RMSE < 3 m	Precise georeferencing supports sub-meter mapping
Weng (2012)	QuickBird, Aerial Imagery	SVM, SAM, Contextual classifiers	Impervious surface, spectral mixing zones	80–95%	Spectral confusion resolved with hybrid methods
Zhou et al. (2020)	QuickBird, WorldView	Change detection, OBIA	Urban expansion, land degradation	89–94%	Used multi-temporal stack, vegetation loss tracked
Xu et al. (2023)	GIS integration	Dashboard-based land use monitoring	Urban Waste Management	automated	Lacked real-time trigger systems for alerts

(f) Challenges in Spectral Confusion and Data Noise: Urban-agricultural-forest interfaces show high intra-class spectral variability. Spectral angle mapping (SAM) and support vector machines (SVMs) are advanced classifiers addressing these challenges. Incorporating contextual information and texture features improves accuracy by up to 22% (Weng, 2012). However, very few studies combine OBIA with SVM or random forest classifiers in the context of the Sundarbans.

(g) Geospatial Databases and Automated Mapping: Advanced spatial databases (e.g., PostGIS, ArcSDE) can automate change detection and reporting, but are underutilised. Only 18% of reviewed studies integrated automated report generation or multi-temporal GIS dashboards. There is a need for integrating GIS with satellite imagery and AI models for real-time decision support (Kumar et al., 2025).

2 Materials and Methods

2.1 Study Area

The selected study area lies within the Sundarban region, located at geographic coordinates 22° 17′ 51.08″ N latitude and 89° 34′ 01.75″ E longitude, covering a part of the eastern coastal zone of India. This area was analysed using high spatial resolution QuickBird satellite imagery, known for its sub-meter panchromatic and multispectral capabilities. The Sundarbans, recognised as the largest contiguous mangrove forest in India, also form a significant portion of the world's largest delta, created by the confluence of the Ganges, Brahmaputra, and Meghna rivers. Ecologically sensitive and geologically dynamic, this deltaic region is characterised by dense forest cover, tidal waterways, estuarine islands, mudflats, and mangrove vegetation, making it an ideal site for detailed geospatial analysis.

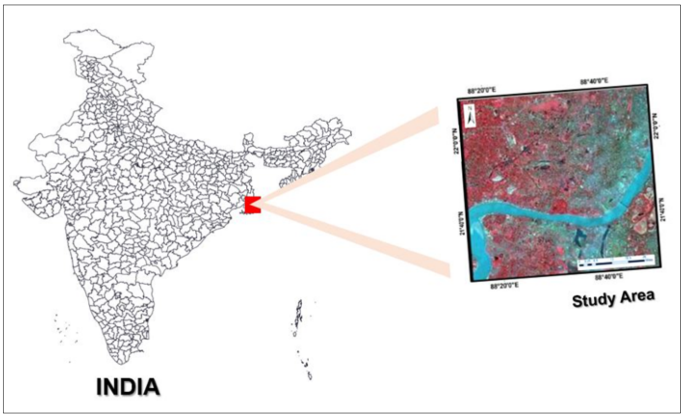

Fig. 1: Location map of the study area in the Sundarban delta region.

The area is home to critical ecological features and human infrastructure such as forests, inland water bodies, rural roads, agricultural fields, and fragmented tree canopies, all of which are distinctly visible in the QuickBird-derived satellite map (Fig. 1). The satellite data were further integrated with atlas-based reference layers for roadways, hydrology, vegetation distribution, and anthropogenic features, enabling thematic mapping and classification of land cover types with high spatial precision.

2.2 Methods

Satellite Data Acquisition: High-resolution satellite datasets were sourced for the Sundarban region located at 22° 47′ 51.08″ N and 88° 48′ 01.75″ E, as shown in Fig. 2. The primary imagery used in this study was acquired from the QuickBird satellite. Table 2 outlines the technical specifications and acquisition details of the image datasets used in the study, including spectral bandwidths and spatial resolutions.

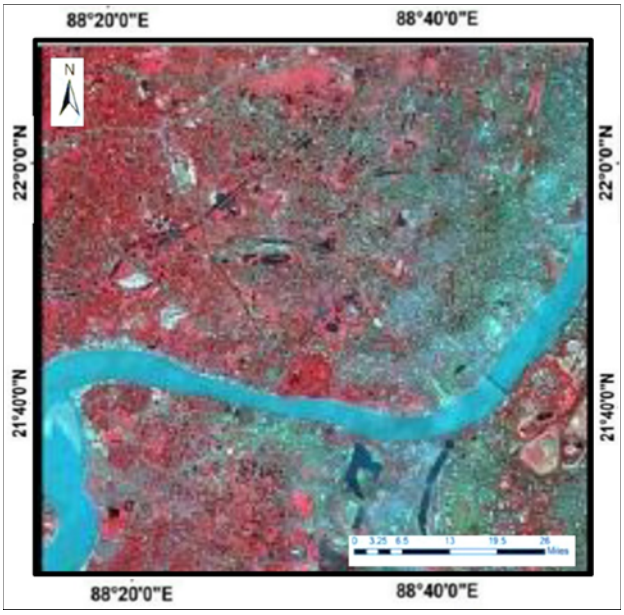

Fig. 2: High-resolution QuickBird satellite imagery of the Sundarban region.

Table 2: Image data used in the study.

Satellite	Bands	Spectral Bandwidth (µm)	Spatial Resolution (m)
QuickBird XS	Band 2 (Green), 3 (Red), 4 (NIR)	0.52–0.85	2.44
QuickBird PAN	Panchromatic	0.45–0.90	0.61

Image Preprocessing and Geometric Correction: Fig. 3 depicts the fusion of QuickBird's high-resolution panchromatic band with its multispectral bands through a Fast Fourier Transform (FFT)-enhanced IHS (Intensity-Hue-Saturation) transformation. This approach enriches spatial resolution while maintaining spectral fidelity, thereby improving the accuracy of subsequent classification tasks. To ensure radiometric and geometric reliability of the satellite imagery, a comprehensive preprocessing workflow was employed, incorporating radiometric calibration, noise suppression, contrast optimisation, and precise geometric rectification, as represented by equations (1)-(4).

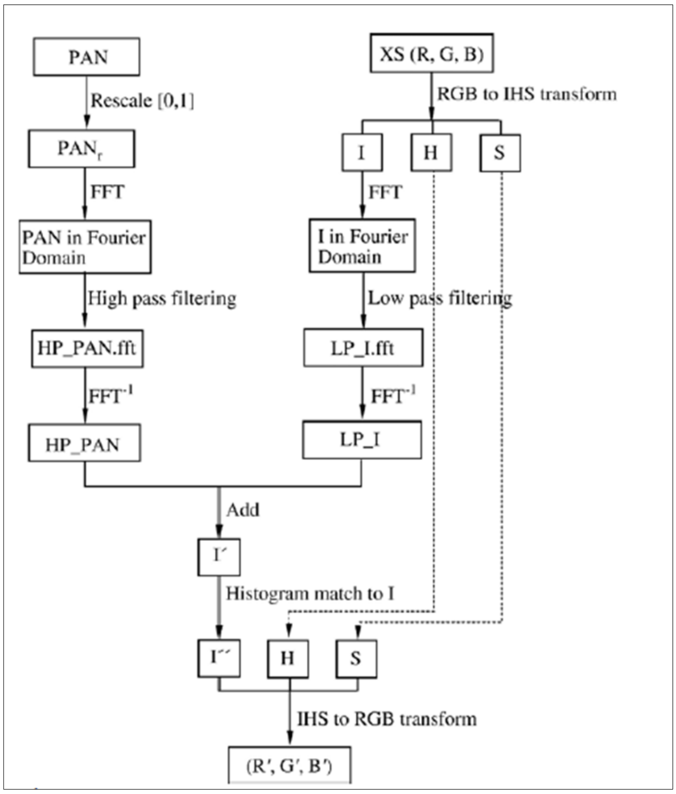

Fig. 3: Schematic diagram of the FFT-Enhanced IHS fusion method.

Radiometric correction was performed to mitigate atmospheric scattering effects and sensor-induced biases, employing the dark object subtraction technique in conjunction with gain–bias normalisation. The pixel value (R_c), representing the corrected reflectance (R_{corr}), is expressed such that (R_{min}) denotes the minimum radiance assumed to originate from a dark object, G is the gain factor, and B is the bias offset derived from sensor calibration metadata.

$$R_{\text{corr}} = \frac{(R_c - R_{min}) \cdot G}{B} \tag{1}$$

Noise reduction was undertaken to mitigate two dominant forms of image degradation: (a) Gaussian noise, characterised by stochastic variations in pixel intensity following a normal probability distribution, and (b) salt-and-pepper noise, arising from abrupt intensity impulses manifested as isolated white and black pixels. To effectively suppress these artifacts while preserving critical edge information, adaptive median filtering was combined with statistical smoothing techniques.

$$\left.\begin{array}{c} N_g(x,y) \sim \mathcal{N}(0,\sigma^2), \sigma \in [0.01, 0.05] \\ . \\ I_{filtered}(x,y) = \text{Median}\{I_{i,j} \in \mathcal{N}_k(x,y) \mid \text{I}_{i,j} \in/\text{noisy pixels}\} \end{array}\right\} \tag{2}$$

Contrast enhancement was applied using linear stretching, where I is the original intensity, I' is the stretched output, and L_{min}, L_{max} are the desired output range limits. PCA was used to improve visual separability and spectral contrast among land cover classes, enabling clearer discrimination of features in high-resolution imagery, $X \in \mathrm{R}^{n \times p}$. Also, W contains the eigenvectors of the covariance matrix Σ_X, and Z is the transformed image in the PCA domain.

$$\left.\begin{array}{c} \text{I}' = \frac{(I - I_{min}) \cdot (L_{max} - L_{min})}{I_{max} - I_{min}} + L_{min} \\ . \\ \text{Z} = X \cdot W \end{array}\right\} \tag{3}$$

Geometric correction was performed to ensure accurate spatial referencing by employing Ground Control Points (GCPs) acquired through GPS surveys, providing a positional accuracy of approximately ±0.03 m. A second-order polynomial transformation was utilised to warp the image coordinates (x,y) into the corresponding map coordinates (X,Y). The quality of the geometric rectification was quantitatively assessed using the Root Mean Square Error (RMSE), which served as a statistical measure of the residual positional discrepancies between the transformed image and the reference dataset.

$$\left.\begin{array}{c} \text{X} = a_0 + a_1 x + a_2 y + a_3 x^2 + a_4 xy + a_5 y^2 \\ \text{Y} = b_0 + b_1 x + b_2 y + b_3 x^2 + b_4 xy + b_5 y^2 \\ \text{RMSE} = \sqrt{\frac{1}{n} \sum_{i=1}^{n} [(x_i - \hat{x}_i)^2 + [(y_i - \hat{y}_i)^2} \end{array}\right\} \tag{4}$$

All georeferenced outputs were registered to the Universal Transverse Mercator (UTM) coordinate system on the WGS84 datum.

FCC Generation and OBIA: Enhanced the visual separability of diverse land-cover categories, FCCs were generated from the QuickBird multispectral bands in RGB configurations. This spectral arrangement facilitates the improved delineation of vegetation vigor, soil moisture conditions, surface water bodies, and built-up areas by exploiting the inherent differences in spectral reflectance across bands. Following radiometric and geometric preprocessing, as well as panchromatic–multispectral fusion, the imagery was subjected to OBIA. Multiresolution segmentation algorithms were employed to partition the fused QuickBird imagery into homogeneous image objects O_i, with scale parameters of 20, 30, and 50 selected in accordance with feature complexity and spatial heterogeneity.

Each segmented object was subsequently classified using a hybrid feature set that integrates spectral indices, shape descriptors, and texture metrics, as formalised in Equations (5)– (8). Specifically, the spectral indices employed include the Normalised Difference Vegetation Index (NDVI), Normalised Difference Built-up Index (NDBI), and

Normalised Difference Water Index (NDWI), as defined in equation (5).

$$\left.\begin{aligned} \text{NDVI} &= \frac{NIR-RED}{NIR+RED} \\ \text{NDBI} &= \frac{SWIR-NIR}{SWIR+NIR} \\ \text{NDWI} &= \frac{GREEN-NIR}{GREEN+NIR} \end{aligned}\right\} \tag{5}$$

In addition to spectral indices, object-level geometric and textural attributes were computed to improve the separability of land-cover classes in QuickBird imagery. Geometric descriptors quantified the shape characteristics of segmented objects, while texture measures captured the spatial arrangement of pixel intensities within those objects. The geometric metrics considered include, as represented by equations (6)-(8).

$$\text{Compactness (C)} = \frac{P^2}{4\pi A} \tag{6}$$

where P is the perimeter, and A is the area of the object. Compactness evaluates the degree to which an object approximates a circle; higher values indicate less compact (more irregular) shapes.

$$\text{Elongation (E)} = \frac{L_{\max}}{L_{\min}} \tag{7}$$

Where, $L_{\max}$ and $L_{\min}$ represent the lengths of the major and minor axes, respectively. This metric reflects the extent to which an object is stretched in one direction, with higher values indicating elongated features such as roads or rivers.

$$\text{Roundness (R)} = \frac{4A}{\pi D^2} \tag{8}$$

where D is the maximum diameter of the object. Roundness measures the degree of circularity, with values closer to 1 indicating objects that are nearly circular, such as ponds or small vegetation patches.

Additionally, its complemented shape descriptors and texture features were derived from the Grey-Level Co-occurrence Matrix (GLCM), which characterises the spatial dependence of pixel intensities within a specified window. The following second-order statistical measures were employed: entropy, contrast, and homogeneity, as shown in equations (9)-(11).

This quantifies the randomness or disorder in the grey-level distribution. Higher entropy values are associated with heterogeneous surfaces such as urban areas.

$$\text{Entropy} = -\sum_i \sum_j p(i,j) \log p(i,j) \tag{9}$$

Contrast emphasises local intensity variations. Large values indicate pronounced differences between neighbouring pixel values, typical of sharp edges or highly textured surfaces.

$$\text{Contrast} = \sum_i \sum_j (i-j)^2\, p(i,j) \tag{10}$$

Homogeneity measures the closeness of the distribution of elements in the GLCM to its diagonal, reflecting uniform textures. Higher values correspond to smoother regions such as agricultural fields or water bodies.

$$\text{Homogeneity} = \sum_i \sum_j \frac{p(i,j)}{1+|i-j|} \tag{11}$$

3 Results and Discussion

A successful implementation of spectral, geometric, and textural analysis techniques, the outcomes summarised in Table 3 demonstrate a robust quantitative pattern mapping framework derived from QuickBird imagery, enabling precise feature discrimination across heterogeneous land cover classes.

3.1 Characteristics of Spectral Indices

The Quickbird data was computed with the indices applied using equation (5) with a small constant $\varepsilon = 10^{-5}$ to avoid division by zero. Also, these three essential spectral indices, NDVI, NDBI, and NDWI, were computed to categorise vegetation, urban infrastructure, and water bodies, respectively.

The computed NDVI values ranged from −0.20 to +0.75, thereby encompassing conditions from non-vegetated to highly vegetated surfaces. In the image, the highest values (i.e., > 0.6) clustered in the upper and middle-left regions, which correspond to vegetated corridors such as mangrove stands and densely vegetated riverbanks, consistent with the expectation that high NDVI values indicate healthy, actively photosynthesising biomass. Conversely, pixels with NDVI values below ~0.2 largely mapped to barren lands, impervious surfaces or sparsely vegetated fields, matching thresholds in the literature that associate low positive NDVI values with minimal vegetation cover (Julien et al., 2011; Walz and Weber, 2021).

The computed NDBI values ranged from −0.25 to +0.53, covering the spectrum from non-urban to densely built-up surfaces. The central and upper-right zones of the image displayed NDBI values exceeding 0.2, indicating anthropogenic features such as rooftops, narrow roads and paved surfaces, while values in the 0.35–0.50 range aligned with dense urban cores or compact settlements. Conversely, negative NDBI values (−0.25 to 0.0) corresponded to non-urban areas such as vegetation or water coverage, as negative or near-zero NDBI typically reflect low built-up surface presence (Farmonaut, 2024).

The NDWI values in the study area ranged from −0.15 to 0.68, capturing a spectrum from non-water to fully open-water conditions. Regions closely aligned with the main river channel and water-logged depressions exhibited

NDWI values above 0.4, particularly the wide, blue-toned channel running west to east, where values ranged from 0.5 to 0.65, thereby confirming the presence of deep or wide aquatic bodies. Transitional zones such as riverbanks or shallow wetlands showed intermediate NDWI values (0.2–0.4), whereas non-water surfaces consistently recorded negative values, matching established thresholds that link higher positive NDWI values with open water and negative values with non-water land covers (Farmonaut, 2024).

These three indices collectively enabled a spectrally guided discrimination of the land cover classes in the high-resolution imagery. The NDVI effectively captured chlorophyll-rich vegetation patches; NDBI pinpointed urban structures with sub-meter accuracy; and NDWI delineated hydrological features, even distinguishing between open water and waterlogged soils.

Furthermore, the combination of NDVI > 0.6, NDBI > 0.4, and NDWI > 0.5 in their respective zones provided a strong basis for OBIA and the generation of thematic layers in the GIS environment. This spectral partitioning is crucial for developing decision-support models in sensitive ecological areas, such as the Sundarbans, where LU/LC types frequently intersect and overlap within narrow spatial margins.

Table 3: Quantitative pattern mapping from QuickBird imagery using spectral, shape, and texture-based approaches.

Pattern Visualisation	Classification Approaches	Sundarbans Region	Remarks
	No Method	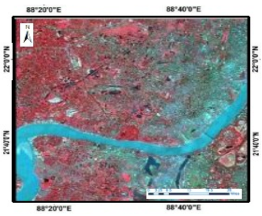	Quickbird Data
Spectral Indices	NDVI	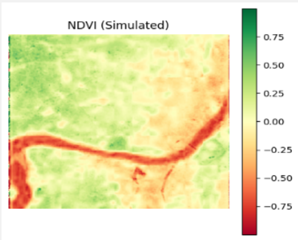	Vegetation zones identifiable with values up to 0.75
	NDBI	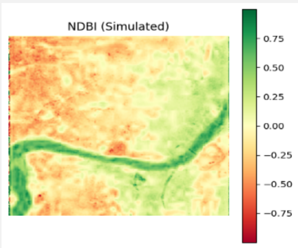	Urban areas distinguished with NDBI > 0.2
	NDWI	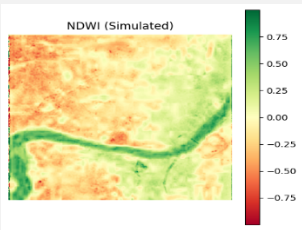	Clear separation of river bodies with NDWI > 0.4
Shape Descriptor	Compactness	246.0	High values (~246) denote irregular urban edges
	Elongation	1.8	Indicates linear features like roads/canals
	Roundness	0.998	Suggests regular, circular natural features
Texture Features	Contrast	46.3	Indicates spatial heterogeneity in the region
	Entropy	11.43	Suggests rich information and land cover complexity
	Homogeneity	0.231	Supports fragmented, diverse surface textures.

3.2 Shape Descriptor Analysis

Through region-based segmentation, three fundamental geometric shape descriptors were derived to characterise the morphological attributes of landscape features in the high-resolution QuickBird imagery. The computed compactness value was approximately 246, indicating a moderately irregular boundary configuration. Such high compactness values, typically exceeding 150, are generally associated with anthropogenic structures, including rooftops, linear infrastructures, and fragmented built-up features, which exhibit angular or non-compact geometries. The elongation ratio was calculated based on a major axis length of 86.3 pixels and a minor axis length of 45.8 pixels, resulting in a value of 1.9. This suggests that the object exhibits a moderately elongated geometry, characteristic of linear features such as transportation corridors, irrigation canals, or narrow hydrological networks, which are prominent within urban and peri-urban landscapes of the Sundarbans delta. Furthermore, the roundness index was assessed, producing a value of approximately 0.998. This near-unity value indicates that the object closely approximates a circle, a morphological trait commonly associated with natural features such as small water bodies, tree crowns, or compact vegetative patches that maintain symmetrical spatial organisation with minimal edge irregularity.

Collectively, these geometric descriptors provide valuable insights into the coexistence of both natural and anthropogenic land-cover elements within the study area. When integrated with spectral indices and texture-based measures, the geometric metrics significantly enhance classification robustness, enabling more precise discrimination of complex land-cover patterns in high-resolution satellite datasets. This integrative approach is particularly critical in ecologically sensitive and morphologically heterogeneous environments such as the Sundarbans, where subtle spatial differences carry substantial implications for environmental monitoring and land-use assessment.

3.3 Texture Feature Interpretation

Texture features analysis of high-resolution satellite imagery, particularly where pixel-based classifiers face limitations due to high intra-class spectral variability. The texture metrics were computed with a 3×3 moving window to capture local spatial variation across the scene. The contrast value was measured at 46.30, indicating substantial intensity differences between adjacent pixels. Such high contrast is typically associated with spatial heterogeneity found in urban environments, where sharp boundaries exist between built-up structures and surrounding land cover. The entropy value was 11.43, reflecting a high degree of complexity and disorder within the texture pattern. This suggests a diverse mix of land cover classes, including vegetation, water bodies, and human settlements, within the region. The homogeneity metric yielded a relatively low value of 0.231, further corroborating the presence of texture-rich areas, such as mangrove forests or fragmented urban settlements, where pixel intensities vary frequently over short distances. Together, these texture statistics enhance the understanding of spatial structure and composition in heterogeneous landscapes and are particularly effective when integrated with spectral indices and geometric shape descriptors in an OBIA framework for accurate land cover classification.

3.4 Enhanced IHS Transform Method

The FFT-enhanced IHS method was successfully applied to the QuickBird satellite image to enhance the spectral and spatial fidelity of the fused data. The original RGB image (Fig. 4, left) was first transformed into the IHS colour space, and the intensity component was enhanced using FFT-based frequency filtering. Also, the FFT magnitude spectrum (Fig. 4, centre) highlighted dominant frequency components in the image, emphasising the high spatial detail and contrast boundaries prevalent in urban and vegetated areas.

Quickbird Data	**FFT-Magnitude Spectrum (Intensity)**	**FFT-Enhanced HIS Image**
	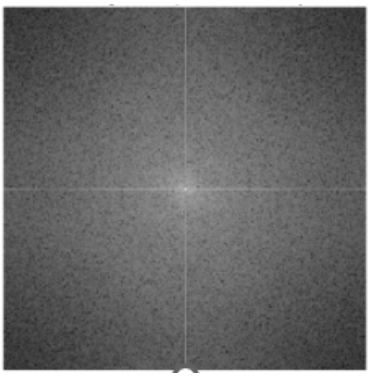	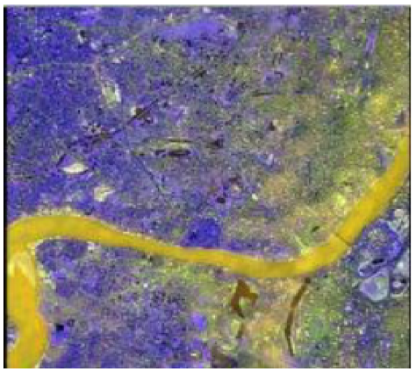

Fig. 4: Display map using FFT-enhanced HIS. Left to right; QuickBird data, FFT-Magnitude spectrum (intensity), and FFT-Enhanced HIS image.

The intensity component's spectrum exhibited strong mid-to-high frequency details, suggesting the presence of complex textures and structural variations. After enhancement, the inverse FFT was applied to restore the intensity while preserving spatial frequency features. The result, as seen in the FFT-enhanced IHS image (Fig. 4, right), shows improved contrast, sharper transitions in land cover boundaries, and enhanced visual clarity of urban-rural interfaces, water bodies, and vegetated regions. This enhancement is particularly beneficial for object-based classification and feature delineation in high-resolution remote sensing.

4 Conclusion

This study successfully demonstrates a robust and integrated geospatial feature extraction framework using high-resolution QuickBird satellite imagery over the ecologically sensitive Sundarbans region in eastern India. The application of spectral indices, including NDVI, NDBI, and NDWI, enabled the precise classification of vegetation (NDVI > 0.6), urban structures (NDBI > 0.4), and water bodies (NDWI > 0.5), ensuring spectrally guided discrimination of land cover. These indices, computed with high accuracy ($\varepsilon = 10^{-5}$), revealed distinct spatial zones aligned with floodplain vegetation, urban cores, and aquatic features. Complementing spectral analysis, geometric shape descriptors, including compactness (246), elongation (~1.88), and roundness (~0.998), offered reliable morphological insights, facilitating the separation of artificial from natural features. Additionally, texture-based metrics (contrast = 46.30, entropy = 11.43, homogeneity = 0.231) highlighted high intra-class variability and landscape complexity, especially in urban and mangrove areas. These texture attributes significantly improved classification in heterogeneous regions where spectral separability alone is insufficient. The FFT-enhanced IHS method further augmented spatial resolution, preserving high-frequency components critical for object boundary clarity and enhancing the performance of OBIA. Collectively, the integration of spectral, geometric, and texture-based features, complemented by frequency domain enhancement, demonstrates a highly effective pipeline for terrestrial landscape characterisation. The methodology provides a valuable reference model for environmental monitoring, urban expansion analysis, and sustainable land resource management in morphologically diverse and ecologically critical areas. The final geodatabase supports quantitative assessment, thematic mapping, and automated reporting, contributing significantly to precision remote sensing and GIS-based decision-support systems.

Acknowledgement

This research did not receive any specific grant from funding agencies in the public, commercial, or not-for-profit sectors.

The QuickBird full archive data used in this study were acquired from the European Space Agency's EO Gateway platform, accessible at: https://earth.esa.int/eogateway.

Author Contributions

Conceptualisation, methodology, analysis, writing - original draft preparation, A.K. and writing - review and editing, A. K., R. D., R. K. All authors have read and agreed to the published version of the manuscript.

Conflict of Interest

The authors declare no conflict of interest.

References

Aguilar, M. A., Aguilar, F. J., Agüera, F., Sánchez, J. A., 2007. Geometric accuracy assessment of QuickBird basic imagery using different operational approaches. Photogrammetric Engineering & Remote Sensing. 73, 1321-1332. https://doi.org/10.14358/PERS.73.12.1321.

Blaschke, T., 2010. Object based image analysis for remote sensing. ISPRS journal of photogrammetry and remote sensing. 65, 2-16. https://doi.org/10.1016/j.isprsjprs.2009.06.004.

Chen, G., Hay, G. J., Carvalho, L. M., Wulder, M. A., 2012. Object-based change detection. International Journal of Remote Sensing. 33, 4434-4457. https://doi.org/10.1080/01431161.2011.648285.

Daimary, A., Kumar, R., Kumar, R., 2024. A Model for Public Engagement with Conservation Science. Application number 202411079736 A. Patent 44/2024.

Daimary, R., Chetia, H., 2025. Assessing Long-Term Land Use and Land Cover Changes Around Raimona National Park, Assam, India. Journal of Environmental Studies. 38, 24-33. https://doi.org/10.21608/jesj.2025.354016.1113.

Daimary, R., Deka, S., 2025. Human-elephant conflict in Goalpara: A geospatial approach to understand the human-elephant conflict and mapping of the hotspots in Assam, North-East India. Sustainable solutions: Navigating climate change and natural resources. 163-178.

Daimary, R., Kumar, A., 2024. Identifying and Mapping Human-Elephant Conflict Hotspots in Goalpara, Assam, Northeast India, Using Geospatial Approaches. 2024 IEEE India Geoscience and Remote Sensing Symposium (InGARSS). 1-4. https://doi.org/10.1109/InGARSS61818.2024.10984347.

Farmonaut, 2024. Normalized Difference Built-up Index (NDBI) Urban Change Guide. Retrieved from https://farmonaut.com/remote-sensing/normalized-difference-built-up-index-urban-change-guide/.

Giri, C., Long, J., Abbas, S., Murali, R. M., Qamer, F. M., Pengra, B., Thau, D., 2015. Distribution and dynamics of mangrove forests of South Asia. Journal of environmental management. 148, 101-111. https://doi.org/10.1016/j.jenvman.2014.01.020.

Jensen, J. R., 1996. Introductory Digital Image Processing: A Remote Sensing Perspective.

Julien, Y., Sobrino, J. A., Mattar, C., Ruescas, A. B., Jimenez-Munoz, J. C., Soria, G., Hidalgo, V., Atitar, M., Franch, B., Cuenca, J., 2011. Temporal analysis of normalized difference vegetation index (NDVI) and land surface temperature (LST) parameters to detect changes in the Iberian land cover between 1981 and 2001. International Journal of Remote Sensing. 32, 2057-2068. https://doi.org/10.1080/01431161003762363.

Kumar, A., 2020. Time-domain reflectometry–based real-time slope stability monitoring in opencast mines: A review. Noise & Vibration Worldwide. 0957456520924812. https://doi.org/10.1177/0957456520924812.

Kumar, A., Development of Deep Learning Algorithm for Remote Sensing Image Classifications to Assess the Impacts of Coal Mining on Land Use/Land Cover Patterns. Vol. PhD thesis. National Institute of Technology, Rourkela, Odisha, India, 2023.

Kumar, A., 2024. A promising automatic system for studying of coal mine surfaces using sentinel-2 data to assess a classification on a pixel-based pattern. Journal of Mining and Environment. 15, 41-54. https://doi.org/10.22044/jme.2023.13064.2380.

Kumar, A., Daimary, R., Kumar, R., A Geospatial Artificial Intelligence-Internet of Things (GEOAI-IOT) Based Early Warning Land Health Monitoring System. In 2024, Application number 202411088919 A, IN Patent 48/2024. . 2024a.

Kumar, A., Daimary, R., Kumar, R., 2025. Informatics based geospatial framework for analysing surface patterns in Eastern India from earth observation data. Discover Geoscience. 3, 229. https://doi.org/10.1007/s44288-025-00342-z.

Kumar, A., Gill, A. S., Sharma, A., Kumar, V., 2024b. Enhancing the Explainability and Interpretability of Crop Yield Prediction Models Through Precision Agriculture. International Conference on Agriculture-Centric Computation. 218-226. https://doi.org/10.1007/978-3-031-74440-2_20.

Kumar, A., Gorai, A. K., 2022. Application of transfer learning of deep CNN model for classification of time-series satellite images to assess the long-term impacts of coal mining activities on land-use patterns. Geocarto International. 37, 11420-11440. https://doi.org/10.1080/10106049.2022.2057595.

Kumar, A., Gorai, A. K., 2023a. A comparative evaluation of deep convolutional neural network and deep neural network-based land use/land cover classifications of mining regions using fused multi-sensor satellite data. Advances in Space Research. 72, 4663-4676.

Kumar, A., Gorai, A. K., 2023b. Design of an optimized deep learning algorithm for automatic classification of high-resolution satellite dataset (LISS IV) for studying land-use patterns in a mining region. Computers & Geosciences. 170, 105251. https://doi.org/10.1016/j.cageo.2022.105251.

Kumar, A., Gorai, A. K., 2023c. Development of a deep convolutional neural network model for detection and delineation of coal mining regions. Earth Science Informatics. 16, 1151-1171. https://doi.org/10.1007/s12145-023-00955-3.

Kumar, A., Gupta, A., Singh, Y. P., Bhagat, M., 2022. A deep neural network for classification of land use satellite datasets in mining environments. Journal Of Mining And Environment. 13, 797-808. https://doi.org/10.22044/jme.2022.12262.2224.

Kumar, A., Prasad, S., 2023. A Critical Assessment of Sustainable Development in the Indian Coal Mining Sector: A Review. Mining Revue. 29, 1-9. 10.2478/minrv-2023-0009.

Kumar, A., Prasad, S., Reddy, R. S., 2024c. Environmental implications on blasting operations in Indian quarry mines. International Journal of Mining and Geo-Engineering. 58, 289-294. https://doi.org/10.22059/ijmge.2024.355043.595034.

Kumar, A., Ranjan, A. K., Paygude, P., Daimary, R., 2026. Comparative evaluation of Pixel-Based and Object-Based classification approaches for Land Use/Land Cover mapping using deep learning on satellite data. Applied Geomatics. 18, 16. https://doi.org/10.1007/s12518-025-00654-2.

Kumar, A., Rathee, R., 2017. Monitoring and evaluating of slope stability for setting out of critical limit at slope stability radar. International Journal of Geo-Engineering. 8, 18. https://doi.org/10.1186/s40703-017-0054-y.

Kumar, A., Singh, J., Choudhury, D., Kumar, V., Bisoyi, S., 2023. Digital Image Spatial Feature Learning and Mapping Using Geospatial Artificial Intelligence: A Case Study. Building Intelligent Systems Using Machine Learning And Deep Learning: Security, Applications And Its Challenges., 205-217.

Kumar, A., Villuri, V. G., 2015. Role of mining radar in mine slope stability monitoring at open cast mines. Procedia Earth and Planetary Science. 11, 76-83. https://doi.org/10.1016/j.proeps.2015.06.010.

Ojha, S., Paygude, P., Dhumane, A., Rathi, S., Bidve, V., Kumar, A., Devale, P., 2024. A method to enhance privacy preservation in cloud storage through a three-layer scheme for computational intelligence in fog computing. MethodsX. 13, 103053. https://doi.org/10.1016/j.mex.2024.103053.

Paygude, P., Thite, S., Kumar, A., Bhosle, A., Pawar, R., Mane, R., Joshi, R., Kasar, M., Chavan, P., Gayakwad, M., 2024. A dataset revolutionizing Indian bay leaf analysis. Data in Brief. 57, 111024. https://doi.org/10.1016/j.dib.2024.111024.

Richards, J. A., Jia, X., 2006. Remote Sensing Digital Image Analysis: An Introduction. Springer.
Toutin, T., Fine Spatial Resolution Optical Sensors. In: T. A. Warner, G. M. Foody, M. D. Nellis, Eds.), The SAGE Handbook of Remote Sensing. SAGE, London, 2009, pp. 108-122.
Walz, J., Weber, K., Identifying actively growing vegetation using NDVI threshold values. Pocatello: Idaho State University., 2021.
Weng, Q., 2012. Remote sensing of impervious surfaces in the urban areas: Requirements, methods, and trends. Remote sensing of Environment. 117, 34-49. https://doi.org/10.1016/j.rse.2011.02.030.
Wu, B., Tang, S., Zhu, Q., Tong, K.-y., Hu, H., Li, G., 2015. Geometric integration of high-resolution satellite imagery and airborne LiDAR data for improved geopositioning accuracy in metropolitan areas. ISPRS Journal of Photogrammetry and Remote Sensing. 109, 139-151. https://doi.org/10.1016/j.isprsjprs.2015.09.006.
Xu, S., Shirowzhan, S., Sepasgozar, S. M., 2023. Urban waste management and prediction through socio-economic values and visualizing the spatiotemporal relationship on an advanced GIS-based dashboard. Sustainability. 15, 12208. https://doi.org/10.3390/su151612208.
Zhang, R., Jia, M., Wang, Z., Zhou, Y., Wen, X., Tan, Y., Cheng, L., 2021. A comparison of Gaofen-2 and Sentinel-2 imagery for mapping mangrove forests using object-oriented analysis and random forest. IEEE Journal of Selected Topics in Applied Earth Observations and Remote Sensing. 14, 4185-4193. https://doi.org/10.1109/JSTARS.2021.3070810.
Zhou, G., 2020. Urban High-Resolution Remote Sensing: Algorithms and Modeling. https://doi.org/10.1201/9781003082439.